Highly Stable Low Redox Potential Quinone for Aqueous Flow Batteries

Min Wu,[1] Meisam Bahari,[1] Yan Jing,[2] Kiana Amini,[1] Eric M. Fell,[1] Thomas Y. George,[1] Roy G.

Gordon,[2]*Michael J. Aziz[1]*

[1] John A. Paulson School of Engineering and Applied Sciences, Harvard University, Cambridge,

Massachusetts 02138, United States

[2] Department of Chemistry and Chemical Biology, Harvard University, Cambridge,

Massachusetts 02138, United States

Corresponding Authors

* gordon@chemistry.harvard.edu; * maziz@harvard.edu

Abstract

Aqueous organic redox flow batteries are promising candidates for large-scale energy storage. However, the design of stable and inexpensive electrolytes is challenging. Here, we report a highly stable, low redox potential, and potentially inexpensive negolyte species, sodium 3,3',3'',3'''-((9,10-anthraquinone-2,6-diyl)bis(azanetriyl))tetrakis(propane-1-sulfonate) (2,6-N-TSAQ), which is synthesized in a single step from inexpensive precursors. Pairing 2,6-N-TSAQ with potassium ferrocyanide at pH 14 yielded a battery with the highest open-circuit voltage, 1.14 V, of any anthraquinone-based cell with a capacity fade rate <10%/yr. When 2,6-N-TSAQ was cycled at neutral pH, it exhibited two orders of magnitude higher capacity fade rate. The great difference in anthraquinone cycling stability at different pH is interpreted in terms of the thermodynamics of the anthrone formation reaction. This work shows the great potential of organic synthetic chemistry for the development of viable flow battery electrolytes and demonstrates the remarkable performance improvements achievable with an understanding of decomposition mechanisms.

Introduction

Safe and economical energy storage technologies are indispensable for the deep penetration of intermittent renewable energies such as photovoltaic and wind electricity.[1-3] Aqueous redox flow batteries are promising candidates for large-scale energy storage compared to other storage devices such as pumped-hydro, flywheel, and lithium-ion batteries, owing to the highly modular configuration, long cycle life, and good safety features.[2, 3] Aqueous vanadium redox flow batteries (VRFBs) have been successfully established by many manufacturers, due to their long cycling life

2

and high-power density.[4] However, cost reductions in VRFBs are anticipated to be difficult due to the abundance of vanadium and its fluctuating price. Consequently, aqueous organic redox flow batteries (AORFBs) are attracting tremendous research interest, as the redox active materials comprising earth abundant elements are potentially inexpensive.[3, 5-7] Additionally, the physical and electrochemical properties of redox organics, such as aqueous solubility, molecular size, molecular net charge, redox potential, and chemical stability could be tailored for improved performance via molecular functionalization.[8, 9]

One drawback of many reported AORFBs, however, is their fast capacity fade because redox organics are susceptible to degradation reactions such as nucleophilic substitution, disproportionation, and tautomerization.[3] To date, various redox-active organics based on quinone,[8-21] viologen,[22-31] phenazine,[32-35] alloxazine,[36] ferrocene[23, 24, 37, 38] and nitroxide radical derivatives[22, 28, 32, 39] have been reported for AORFBs. Most of them, however, exhibit high capacity fade rates of 0.1%–1%/day,[3] which is unsuitable for practical application. Recently, anthraquinone derivatives such as 2,6-DBEAQ, 2,6-DPPEAQ, DPivOHAQ and DBAQ have demonstrated very good long-term stability.[11, 16, 19] However, their widespread application is hindered by the high synthetic cost due to sophisticated synthesis or expensive precursors involved. Additionally, there is an apparent trade-off between anthraquinone cycling stability and the redox potential.[40] The highly stable anthraquinones such as 2,6-DBEAQ, DPivOHAQ, and DBAQ have a redox potential more positive than -0.52 V vs. standard hydrogen electrode (SHE) at pH 12 and

above; anthraquinones with a more negative redox potential exhibited less stable cycling performance.[8, 41] For a negolyte molecule, however, a low redox potential is desired to achieve high cell voltage. Therefore, developing inexpensive and stable anthraquinone negolytes with a low redox potential remains crucial for the practical implementation of AORFBs.

Here, we report a potentially inexpensive and low redox-potential anthraquinone negolyte with outstanding cycling stability. The anthraquinone sodium 3,3',3",3'"-((9,10-anthraquinone-2,6-diyl)bis(azanetriyl))tetrakis(propane-1-sulfonate) (2,6-N-TSAQ) was synthesized from inexpensive 2,6-diaminoanthraquinone (2,6-DAAQ) via a one-step N-alkylation route. The redox potential of 2,6-N-TSAQ at pH 12 and above is -0.62 V vs. SHE, which is 120 mV lower than that of the oxygen-linked anthraquinone sodium 3,3'-((9,10-anthraquinone-2,6-diyl)bis(oxy))bis(propane-1-sulfonate) (2,6-O-DPSAQ) and 170 mV lower than that of the carbon-linked anthraquinone sodium 3,3'-(9,10-anthraquinone-2,6-diyl)bis(propane-1-sulfonate) (2,6-DPSAQ). Pairing with ferro/ferricyanide, it yields a cell with an open circuit potential of 1.14 V and a peak power density of 0.18 W/cm^2 at pH 14. The capacity fade rate of 2,6-N-TSAQ is 0.025%/day at pH 14, yielding the highest open-circuit voltage of any anthraquinone-based cell with a capacity fade <10%/yr. Greater capacity fade rates by up to two orders of magnitude at near-neutral pH are interpreted in terms of changes in the driving free energy for anthrone formation. These results provide guidance for improving the performance of anthraquinone negolytes and highlight the great potential of organic synthesis towards inexpensive and stable

72   electrolytes for grid-scale energy storage application.

73

74   **2. Results and Discussion**

75   **Figure 1** illustrates the synthetic routes for three different anthraquinones 2,6-N-TSAQ, 2,6-O-

76   DPSAQ and 2,6-DPSAQ. The structure of 2,6-N-TSAQ was verified by ^{1}H nuclear magnetic

77   resonance (NMR) and high-resolution liquid chromatography-mass spectrometry as shown in

78   **Figure S1** and **S2**. The structures of 2,6-O-DPSAQ and 2,6-DPSAQ were verified by ^{1}H NMR as

79   shown in **Figure S3** and **S4**. Among them, 2,6-N-TSAQ and 2,6-O-DPSAQ were synthesized via

80   similar one-step nucleophilic substitution reactions. 2,6-N-TSAQ was produced from 2,6-DAAQ,

81   and 2,6-O-DPSAQ was synthesized from 2,6-dihydroxyanthraquinone (2,6-DHAQ). In both cases,

82   sodium hydride was used to fully deprotonate the anthraquinone precursors in anhydrous dimethyl

83   sulfoxide or N, N-dimethylformamide. Afterward, the deprotonated anthraquinone precursors

84   react with 1,3-propanesultone overnight at room temperature to afford 2,6-N-TSAQ or 2,6-O-

85   DPSAQ. Benefiting from the high reactivity of 1,3-propanesultone, the reaction is readily

86   performed at room temperature with high purity and yield, making it very suitable for mass

87   production. In contrast, 2,6-DPSAQ was synthesized from 2,6-DAAQ with three steps.[42] First,

88   2,6-DAAQ was converted to 2,6-diiodoanthraquinone. Afterward, it reacted with sodium

89   allylsulfonate via Heck reaction followed by a hydrogenation step to yield 2,6-DPSAQ. The three-

90   step reaction involving precious metal catalysts makes it less attractive compared with the one-

91   step synthesis of 2,6-N-TSAQ and 2,6-O-DPSAQ. Since the laboratory cost of precursor 2,6-

92   DAAQ is much lower than that of 2,6-DHAQ (**Table S1**), 2,6-N-TSAQ could be the most

93   inexpensive anthraquinone among the three at a mass production scale, decreasing the capital cost

94   of AORFBs.
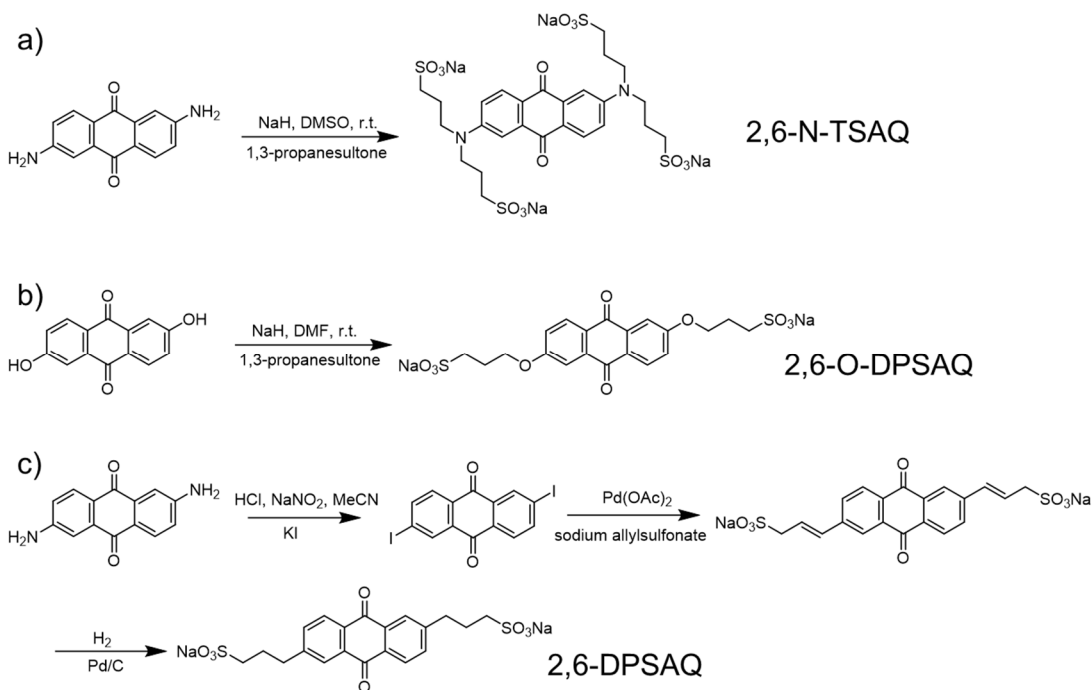
95

96   **Figure 1.** Synthetic routes for three different anthraquinones. a) 2,6-N-TSAQ; b) 2,6-O-DPSAQ;

97   c) 2,6-DPSAQ.

98

99   **Figure 2**a exhibits the cyclic voltammograms (CV) of 2,6-DPSAQ, 2,6-O-DPSAQ, and 2,6-

100   N-TSAQ. The redox potential of 2,6-N-TSAQ is -0.62 V vs. SHE in 1 M NaCl, which is 120 mV

101   and 170 mV lower than that of 2,6-O-DPSAQ and 2,6-DPSAQ in 1 M NaCl, respectively. The low

102   redox potential of 2,6-N-TSAQ is attributed to the strong electron donating effect of nitrogen lone

103   pairs. It contributes to form a high working voltage and high-power density flow battery. The CV

104   of 2,6-N-TSAQ in 1 M NaOH is shown in Figure S5. The redox potential of 2,6-N-TSAQ at pH

105 14 is -0.63 V vs. SHE, which is close to that in 1 M sodium chloride medium. But the peak

106 separation of 2,6-N-TSAQ in 1 M NaOH (94 mV) is much smaller than that in 1 M NaCl (130

107 mV), indicating a much faster redox process at pH 14 than that at lower pH. The water solubility

108 of 2,6-DPSAQ, 2,6-O-DPSAQ, and 2,6-N-TSAQ is shown in **Figure 2**b. Surprisingly, 2,6-O-

109 DPSAQ exhibited an extremely low solubility of 10 mM in deionized water and in 1 M lithium

110 chloride, and an even lower solubility of less than 5 mM in 1 M sodium chloride. The solubilities

111 of 2,6-DPSAQ and 2,6-N-TSAQ in deionized-water (no supporting salt) are 0.3 M and 0.45 M,

112 respectively.
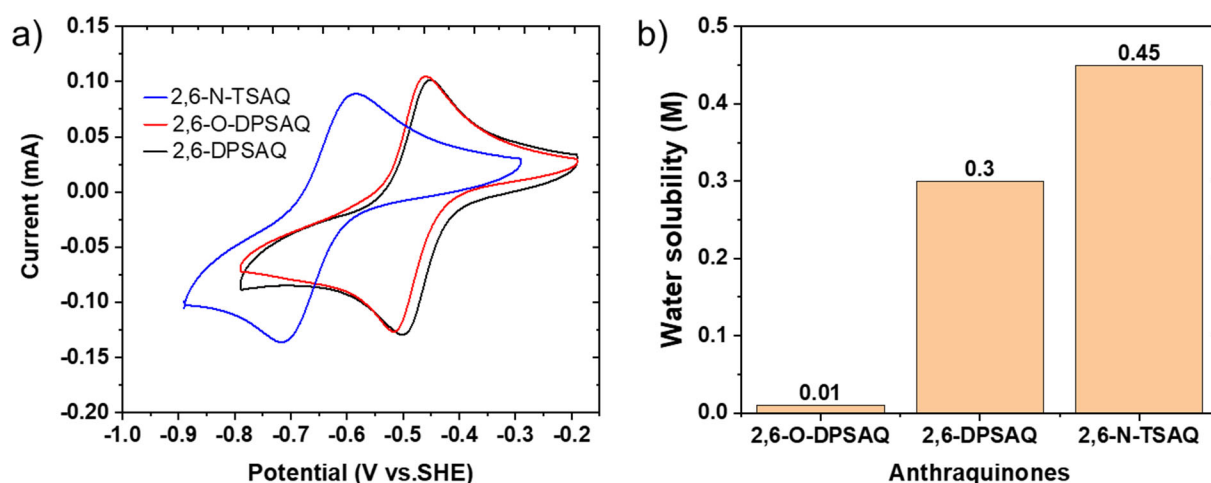
113

114 **Figure 2.** a) Cyclic voltammograms of 5 mM 2,6-N-TSAQ and 5 mM 2,6-DPSAQ in 1 M sodium

115 chloride, and 5 mM 2,6-O-TSAQ in 1 M lithium chloride, each with a scan rate of 100 mV/s; b)

116 Solubility comparison for 2,6-N-TSAQ, 2,6-O-DPSAQ and 2,6-DPSAQ in deionized water.

117

118   Given the higher water solubility, lower redox potential, and possible lower synthetic cost,

119 2,6-N-TSAQ was selected for further electrochemical study. The advantage of 2,6-N-TSAQ over

120 some other low redox potential anthraquinones[8, 41] is that it has four negative charges on the

121 solubilizing groups, leading to a high intermolecular Coulomb repulsion and a low collision rate.

122 According to Marcus theory,[43, 44] these properties could decrease the reaction rate of the

123 disproportionation (known to cause capacity decay in anthraquinone negolyte).[19, 40] The large

124 Coulomb repulsion and bulky functionalization also decrease the molecular permeability across

125 cation exchange membranes, increasing the cell lifetime. The permeability of 2,6-N-TSAQ

126 through sodium-exchanged Nafion NR212 was measured in a two-compartment diffusion cell.

127 Due to a very low crossover rate, we estimate a maximum permeability of 3 x 10^{-14} cm^2/s (Figures

128 S6 and S7), which is even lower than that reported for the tetra-anionic anthraquinone derivative

129 2,6-DPPEAQ.[16]

130 The Pourbaix diagram of 2,6-N-TSAQ, shown in **Figure 3**a, indicates the molecule undergoes

131 a two-proton/two-electron process below pH 10, a one-proton/two-electron process over pH 10–

132 12, and a pH-independent two-electron process at pH > 12 with a redox potential around -0.63 V

133 vs. SHE. The corresponding CV profiles at various pH are shown in Figure S8. It should be noted

134 that the pH is the local pH of anthraquinone molecules. For an unbuffered case, *e.g.*, 1 M NaCl,

135 the formal potential of 2,6-N-TSAQ is -0.62 V, which is close to the redox potential at high pH;

136 such a phenomenon was also observed in other anthraquinones when a pH buffer was not used.[16,

137 [17] Based on the Pourbaix diagram, the pKa1 and pKa2 of reduced and protonated 2,6-N-TSAQ are

138 estimated to have values around 10 and 12, respectively, which are slightly larger than those of

139 anthraquinone negolytes with more positive redox potentials.[9, 11, 16, 19] We attribute this to the strong

140 electron donating effect of lone pair electrons on nitrogen atoms decreasing the p*K*a of hydroxy

141 groups of the 9,10-dihydroxyanthracene (reduced state of anthraquinone).
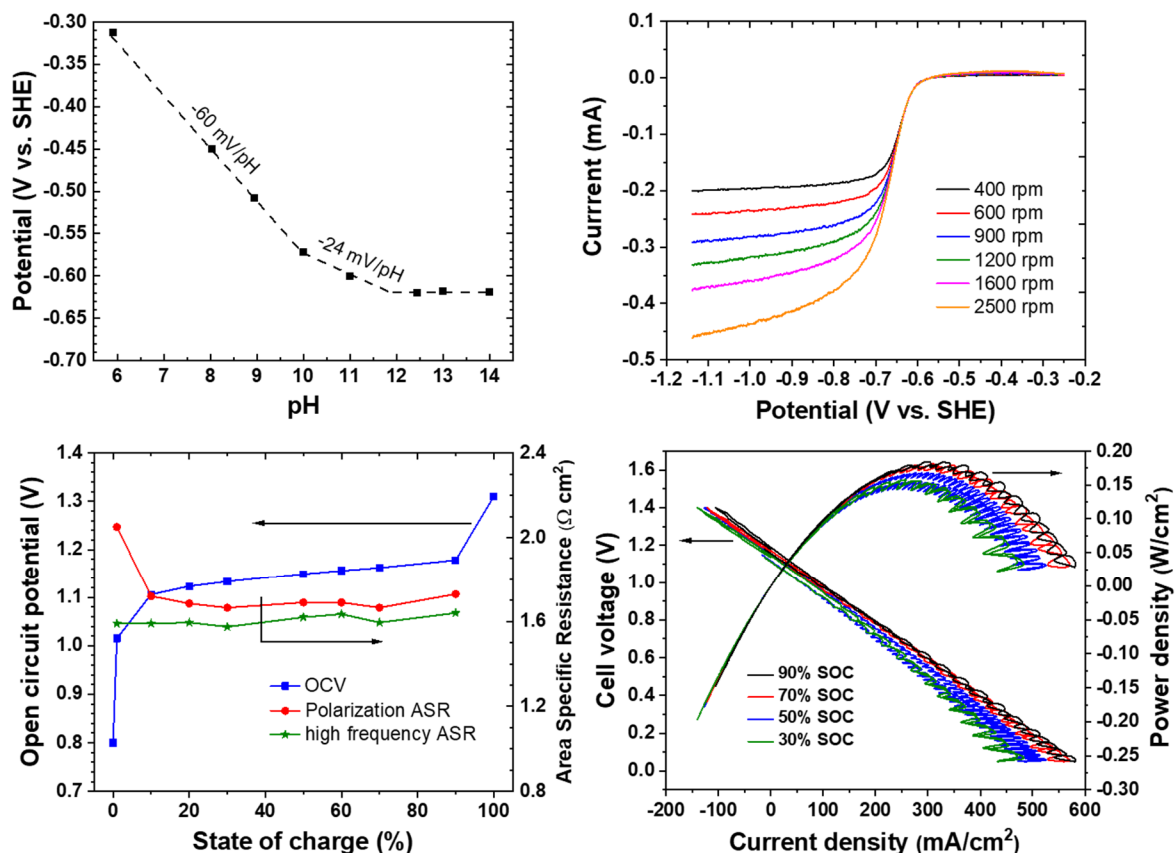
Figure 3. Electrochemical performance of 2,6-N-TSAQ. a) Pourbaix diagram of 2,6-N-TSAQ redox process; b)

Linear sweep voltammograms of 5 mM 2,6-N-TSAQ in 1 M NaOH on a glassy carbon rotating disk electrode

at rotation rates between 400 and 2500 rpm; c) Open circuit voltage (OCV), high-frequency area-specific

resistance (ASR) and polarization ASR versus SOC of 2,6-N-TSAQ/potassium ferrocyanide full cell at pH 14;

d) Polarization measurements of 2,6-N-TSAQ/potassium ferrocyanide full cell at pH 14. Cell configuration in

(c) and (d): 5 mL of 0.1 M 2,6-N-TSAQ pH 14 | 30 mL of 0.1 M $K_4Fe(CN)_6$, 0.02 M $K_3Fe(CN)_6$, pH 14 (1M

NaOH). Sodium exchanged Nafion[®] 212 was used as the ion-selective membrane between the AvCarb carbon

cloth electrodes.

The electrochemical properties of 2,6-N-TSAQ were determined by rotating disk electrode (RDE) test as shown in **Figures 3**b and **S9**. The diffusion coefficient (D) was calculated to be 5.8×10^{-7} cm^2/s by the Levich equation. The charge transfer coefficient was determined to be 0.32 based on the Tafel equation, and the electron transfer rate constant was determined to be 2.53×10^{-4} cm s^{-1}.

Polarization experiments of a 0.1 M 2,6-N-TSAQ/ferrocyanide full cell at pH 14 were performed at various states of charge. The electrolytes comprised 5 mL of 0.1 M 2,6-N-TSAQ (negolyte) at pH 14 and 30 mL of 0.1 M potassium ferrocyanide and 0.02 M potassium ferricyanide (posolyte) at pH 14 to ensure that the negolyte was always the capacity limiting side. The cell was constructed from graphite flow plates and AvCarb carbon cloth electrodes, separated by a Nafion 212 membrane ion exchanged in 1 M NaOH for over 12 hours at room temperature. The electrolyte was charged/discharged at 40 mA/cm^2 between 0.6 V and 1.4 V with a potential hold until the current dropped to 2 mA/cm^2 to get the full capacity. The OCV increased from 0.8 to 1.31 V as the SOC increased from ~0% to ~100% (**Figure 3**a). The 0.2 V increase of OCV from 0 to ~1% SOC, 0.09 V increase from ~1% to ~10%, 0.08 V increase from 10% to 90% SOC, and 0.14 V from 90% to final OCV, indicates the utilization of 2,6-N-TSAQ is more than 99% under the operating conditions according to the Nernst equation. The peak galvanic power density at 10% SOC was 0.15 W cm^{-2} and increased to 0.18 W cm^{-2} at 90% SOC (Figure 3d). The power density is mainly limited by the high-frequency ASR, which is dominated by the membrane resistance (**Figure 3**c) with a value around 1.6 $\Omega\cdot$cm^2. Therefore, the power density is expected to be improved with a

171 lower-resistance membrane.

172   A long-term cycling test of the 0.1 M 2,6-N-TSAQ/ferrocyanide flow battery at pH 14 was

173 performed with the same cell. The cell was cycled at 40 mA cm^{-2} with potential holds at 1.4 V for

174 charging and 0.6 V for discharging until the current density dropped to 2 mA cm^{-2}. The initial

175 volumetric discharge capacity was 4.76 Ah/L, corresponding to a capacity utilization of 88.9% of

176 the theoretical value. However, the OCV at different SOCs in **Figure 3**c and the typical voltage

177 profile in **Figure 4**c indicates it achieves full capacity of 2,6-N-TSAQ under such conditions. The

178 difference between realized capacity and the theoretical value could come from errors in

179 electrolyte volume measurement or the presence of non-redox active impurities such as water or

180 salts in the sample. After 9 days of full SOC range cycling, the discharge capacity decreased to

181 4.75 Ah/L, corresponding to a temporal capacity fade rate of 0.025%/day or 0.00024%/cycle. The

182 average coulombic efficiency was determined to be above 99.9%. The voltage/capacity profile at

183 different cycles in **Figure 4**c are almost invariant, indicating the highly-stable cell performance of

184 2,6-N-TSAQ at pH 14. This high cycling stability is achieved in an anthraquinone molecule with

185 an   unusually   low   redox   potential.
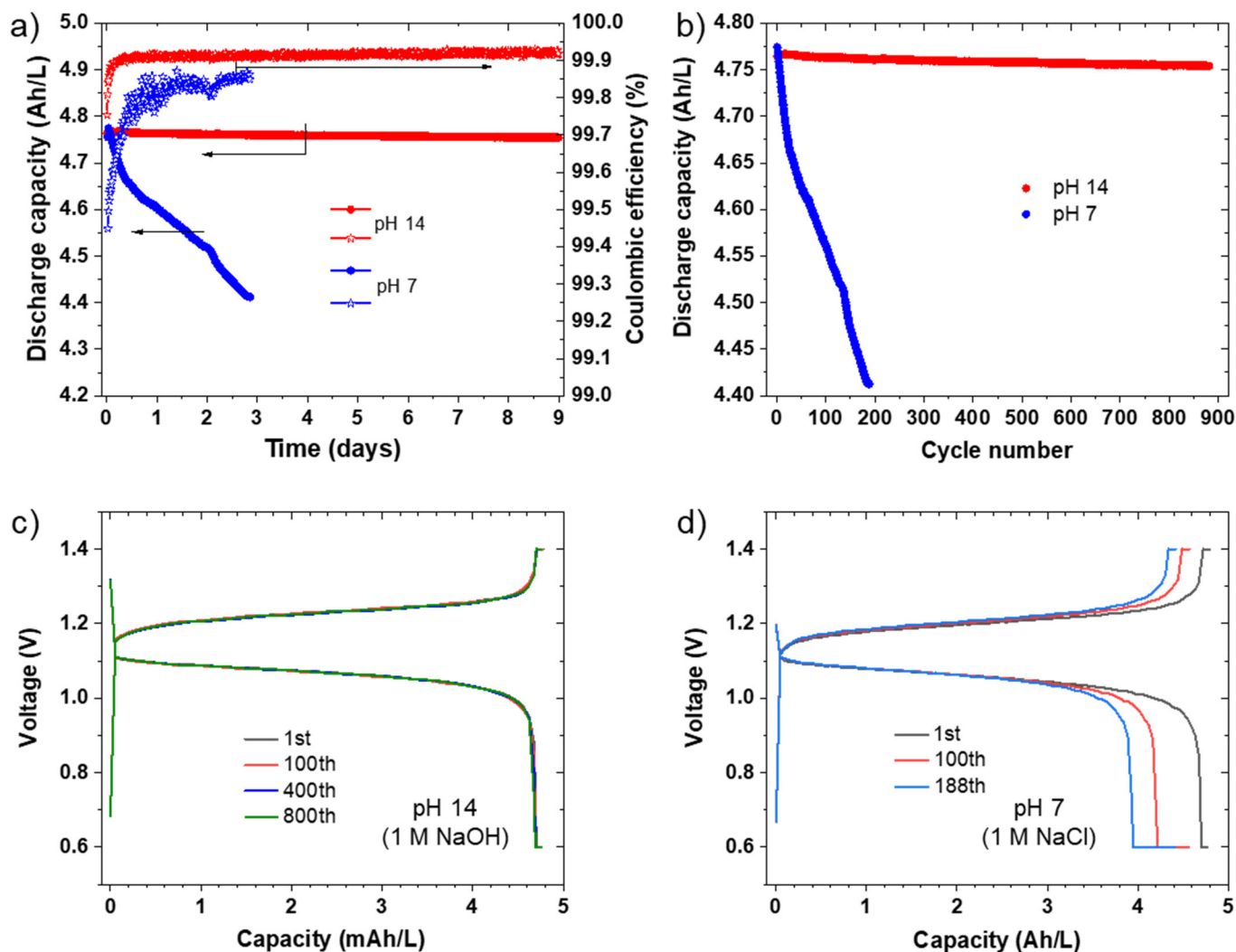
Figure 4. Cell performance of 0.1 M 2,6-N-TSAQ/ferrocyanide cell, 2,6-N-TSAQ as the capacity limiting side. a) Discharge capacity and Coulombic efficiency versus cycle time at pH 7 and 14; b) Discharge capacity versus cycle number at pH 7 and 14; c) Charge-discharge voltage profile of 2,6-N-TSAQ from selected cycles at pH 14 in Figure 4b; d) Charge-discharge voltage profile of 2,6-N-TSAQ from selected cycles at pH 7 in Figure 4b. Untreated AvCarb carbon cloth was used as the electrodes, and sodium or ammonium exchanged Nafion® 212 was the ion-selective membrane.

194   The 0.1 M 2,6-N-TSAQ/ferrocyanide cell under neutral conditions (1 M NaCl) was cycled

195 under the same electrolyte volume, cut-off voltage and current for comparison. The initial

196 volumetric capacity was 4.77 Ah/L and after 2.84 days cycling, the discharge capacity dropped to

197 4.41 Ah/L, corresponding to a capacity fade rate of 2.6%/day, which is around 2 orders of

198 magnitude higher than that at pH 14. The coulombic efficiency was around 99.8% over the whole

199 cycling process, which is slightly lower than that at pH 14. Additionally, as shown in **Figure S10**,

200 the discharge capacity from the constant potential hold at 0.6 V increases and round-trip energy

201 efficiency decreases as the cycle count increases.

202   An otherwise-identical 0.1 M 2,6-N-TSAQ/ferrocyanide full cell was cycled in 1 M NH$_4$Cl

203 enabling the pH to remain below 10 over the entire SOC range. The initial charge capacity was up

204 to 4.98 Ah/L but the initial discharge capacity was only 0.50 Ah/L with a low coulombic efficiency

205 of 10.1% as shown in **Figure S11**. The discharge capacity dropped to 0.29 Ah/L in the third cycle

206 with a coulombic efficiency around 80%. The ^{1}H NMR spectrum for the cycled 2,6-N-TSAQ

207 (NH$_4^+$) is shown in **Figure S12**. The five peaks with asterisks in the aromatic region are similar to

208 the anthrone peaks observed in 2,6-DHAQ,[40] suggesting that the major decomposition of 2,6-N-

209 TSAQ came from anthrone formation. After the electrolyte was fully oxidized by exposure to air,

210 the five peaks with asterisks disappeared and some new peaks appeared, suggesting that the

211 anthrone was oxidized to anthraquinone and anthrone dimer.[19, 40] Furthermore, mass spectrometry

212 was used to analyze the cycled 2,6-N-TSAQ (NH$_4^+$) electrolyte, and anthrone was detected as the

213 major decomposition compound (**Figure S13**).

To investigate the origin of cycling instability of 2,6-N-TSAQ under neutral conditions, both oxidized and reduced forms of 2,6-N-TSAQ were stored in 1 M NaCl at 45 °C for 8 days. No apparent decomposition was found in the ^{1}H NMR of the oxidized state in **Figure S14**. In contrast, the reduced 2,6-N-TSAQ sample showed a large quantity of decomposition after 1 week, implying that the reduced form of 2,6-N-TSAQ undergoes the disproportionation reaction, which is well-known in anthraquinone negolytes, at pH 7. In contrast, only a minor amount of decomposition was detected for the reduced sample when the reduced 2,6-N-TSAQ was stored in 1 M NaOH at 45 °C for 8 days.

We interpret the substantial difference in the stability of reduced anthraquinone at pH 7 and 14 in terms of the thermodynamics of anthrone formation. The disproportionation reaction of 9,10-dihydroxyanthracene is the sum of half reactions I and II in Figure 5a. The Gibbs free energy change $\Delta G^{\circ}{}'$ of the disproportionation reaction under standard conditions except that the pH is fixed at a certain value can be expressed as $\Delta G^{\circ}{}' = -2 \times F \times (E_2 - E_1)$, where E_1 and E_2 are the redox potentials of the two half-reactions under these conditions. The proposed Pourbaix diagram of anthraquinone, 9,10-dihydroxyanthracene, and anthrone is shown in **Figure 5**b. The state of protonation of the molecules on the left-hand side of Reactions I and II is illustrated in the intermediate-potential band of the Pourbaix diagram. When the local pH < pKa1, both half reactions undergo a two-proton/two-electron process. When the local pH is between pKa1 and pKa, reaction I undergoes a one-proton/two-electron process, and reaction II undergoes a three-proton/two-electron reaction. When pKa < pH < pKa2, reaction I still experiences one-proton/two-

234   electron process, while reaction II undergoes a two-proton/two-electron process. When pH is

235   above pKa2, half reaction I becomes pH independent, and half reaction II undergoes a three-

236   proton/two-electron reaction. As shown in **Figure 5**b, the Gibbs free energy change for anthrone

237   formation is around $\Delta(\Delta G^{\circ\prime}) = -2 \times \frac{96485C}{mol} \times \frac{-\frac{0.089 \text{ V}}{pH} \times 2pH}{1000} = 34$ kJ/mol less negative at pH 14

238   than that at pH 12. Similarly, the difference in Gibbs free energy change per mole of anthrone

239   formation at pH 14 and 10 could be as large as $-2 \times 96485 \times (0.089 \times 3 + 0.0295 \times 1)/1000 =$

240   57 kJ/mol, if pKa is around 10 and pKa$_2$ is around 11. Therefore, anthrone formation becomes

241   significantly more disfavored at pH 14 than that at a significantly lower pH. Consequently, when

242   anthrone formation is the predominant decomposition mechanism, anthraquinone-based flow

243   batteries exhibit better cycling performance at high pH than that at lower pH. Moreover, the Gibbs

244   free energy change for the anthrone formation reaction at a 100% SOC (no anthrone and

245   anthraquinone, 100% 9,10-dihydroxyanthracene) is always negative, indicating that for any given

246   anthraquinone, the disproportionation reaction at the full SOC is always thermodynamically

247   favorable. When the SOC of anthraquinone increases from 90% to 99%, the Gibbs free energy

248   change   for   anthrone   formation   becomes   more   negative   by   approximately

249    $8.314 \text{ J/mol/K} \times 298.15 \text{ K} \times (\ln \frac{0.1}{0.9^2} - \ln \frac{0.01}{0.99^2}) = 6.18$ kJ/mol assuming the variation of anthrone

250   concentration is negligible. Likewise, when the SOC of anthraquinone negolyte increases from 90%

251   to 99.9%, the Gibbs free energy change for anthrone formation becomes more negative by

252   approximately 11.93 kJ/mol. Therefore, to suppress anthrone formation in practical deployment,

253   charging to a high SOC should be avoided, i.e., it is desired not to conduct a potential hold at the

15

end of the charging half-cycle. A simple galvanostatic cycling protocol, however, cannot be used in research to evaluate very low capacity fade rates. [3, 45]. For future research on anthraquinone negolytes species, a potential hold after, say, every 30 cycles of galvanostatic cycling might be advisable.
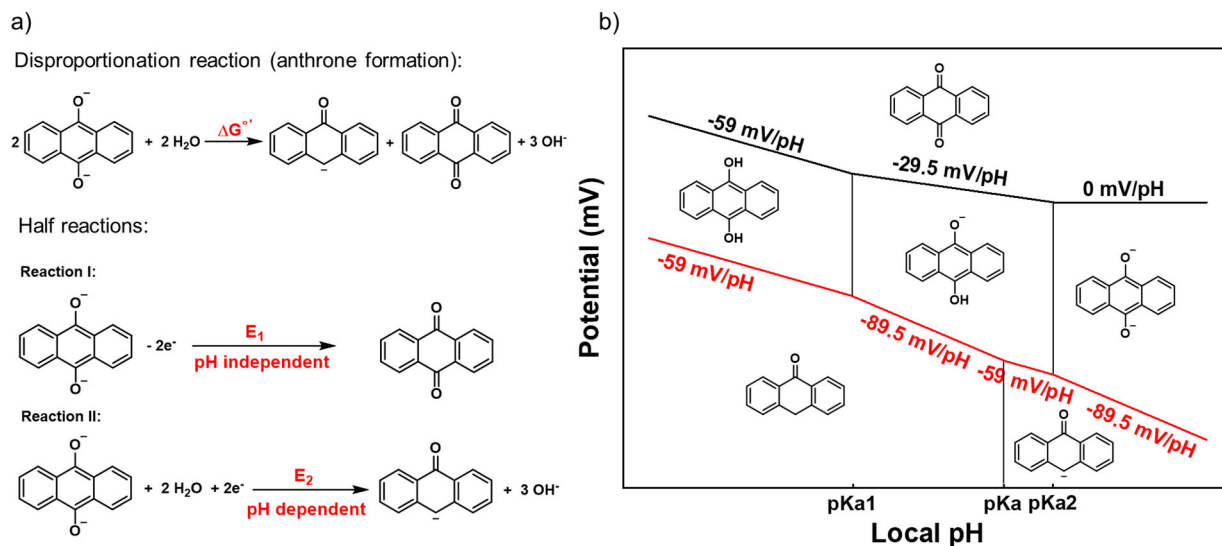
Figure 5. a) Disproportionation reaction of 9,10-dihydroxyanthraceen at pH above its pKa2 and the corresponding two half reactions; b) Representative Pourbaix diagram of anthraquinone, 9,10-dihydroxyanthracene, and anthrone. The pKa_1 and pKa_2 belong to 9,10-dihydroxyanthracene, and pKa (around 10) belongs to anthrone.[46] The water molecules in the half reactions were neglected in Figure 5b due to the space limitation.

In summary, we synthesized three sulfonated anthraquinone derivatives, carbon-linked, nitrogen-linked, and oxygen-linked. The nitrogen-linked anthraquinone (2,6-N-TSAQ) showed a much lower redox potential than the others due to the strongest electron donating effect of lone pair electrons on nitrogen atoms. Because it is synthesized from inexpensive precursor with a one-

16

step N-alkylation method, the mass production cost could be low. Despite the Coulomb repulsion

afforded by its four negatively charged sulfonate groups, the cycling performance of 2,6-N-TSAQ

is poor at neutral pH, with a capacity fade rate of 2.6%/day. The cycling stability improved by two

orders of magnitude to 0.025%/day by raising the pH to 14. The 2,6-N-TSAQ | ferro/ferricyanide

cell at pH 14 exhibits the highest open-circuit voltage, 1.14 V, of any anthraquinone-based cell

with a capacity fade rate no greater than <10%/yr. The great difference in anthraquinone cycling

stability at different pH values is explained in terms of the thermodynamics of anthrone formation.

This work demonstrates the significant improvement in performance that can be made with a better

understanding of capacity fade mechanisms and illustrates the great potential of organic synthetic

chemistry for low-cost and stable AORFB electrolytes.

Supporting Information. The Supporting Information is available free of charge at

CONFLICT OF INTERESTS

285 M.B., R.G.G. and M.J.A. have ownership stakes in Quino Energy, Inc., which may profit from

286 the results reported here.

287

References

1. Dunn, B.;   Kamath, H.; Tarascon, J. M., Electrical energy storage for the grid: a battery of choices. *Science* **2011,** *334* (6058), 928-35.

2. Soloveichik, G. L., Flow Batteries: Current Status and Trends. *Chem Rev* **2015,** *115* (20), 11533-58.

3. Kwabi, D. G.;   Ji, Y.; Aziz, M. J., Electrolyte lifetime in aqueous organic redox flow batteries: A critical review. *Chem Rev* **2020,** *120* (14), 6467–6489.

4. Ulaganathan, M.;   Aravindan, V.;   Yan, Q.;   Madhavi, S.;   Skyllas-Kazacos, M.; Lim, T. M., Recent Advancements in All-Vanadium Redox Flow Batteries. *Advanced Materials Interfaces* **2016,** *3* (1), 1500309.

5. Luo, J. A.;   Hu, B.;   Hu, M. W.;   Zhao, Y.; Liu, T. L., Status and Prospects of Organic Redox Flow Batteries toward Sustainable Energy Storage. *ACS Energy Letters* **2019,** *4* (9), 2220-2240.

6. Winsberg, J.;   Hagemann, T.;   Janoschka, T.;   Hager, M. D.; Schubert, U. S., Redox-Flow Batteries: From Metals to Organic Redox-Active Materials. *Angew Chem Int Ed* **2017,** *56* (3), 686-711.

7. Wei, X. L.;   Pan, W. X.;   Duan, W. T.;   Hollas, A.;   Yang, Z.;   Li, B.;   Nie, Z. M.;   Liu, J.;   Reed, D.;   Wang, W.; Sprenkle, V., Materials and Systems for Organic Redox Flow Batteries: Status and Challenges. *ACS Energy Letters* **2017,** *2* (9), 2187-2204.

8. Lin, K.;   Chen, Q.;   Gerhardt, M. R.;   Tong, L.;   Kim, S. B.;   Eisenach, L.;   Valle, A. W.;   Hardee, D.;   Gordon, R. G.;   Aziz, M. J.; Marshak, M. P., Alkaline quinone flow battery. *Science* **2015,** *349* (6255), 1529-32.

9. Huskinson, B. T.;   Marshak, M. P.;   Suh, C.;   Er, S.;   Gerhardt, M. R.;   Galvin, C. J.;   Chen, X.;   Aspuru-Guzik, A.;   Gordon, R. G.; Aziz, M. J., A metal-free organic-inorganic aqueous flow battery. *Nature* **2014,** *505* (7482), 195-8.

10. Gerhardt, M. R.;   Tong, L.;   Gomez-Bombarelli, R.;   Chen, Q.;   Marshak, M. P.;   Galvin, C. J.;   Aspuru-Guzik, A.;   Gordon, R. G.; Aziz, M. J., Anthraquinone Derivatives in Aqueous

Flow Batteries. *Advanced Energy Materials* **2017,** *7* (8), 1601488.

11. Kwabi, D. G.;　Lin, K.;　Ji, Y.;　Kerr, E. F.;　Goulet, M.-A.;　De Porcellinis, D.;　Tabor, D. P.;　Pollack, D. A.;　Aspuru-Guzik, A.;　Gordon, R. G.; Aziz, M. J., Alkaline quinone flow battery with long lifetime at pH 12. *Joule* **2018,** *2* (9), 1907-1908.

12. Cao, J. Y.;　Tao, M.;　Chen, H. P.;　Xu, J.; Chen, Z. D., A highly reversible anthraquinone-based anolyte for alkaline aqueous redox flow batteries. *Journal of Power Sources* **2018,** *386*, 40-46.

13. Yang, Z.;　Tong, L.;　Tabor, D. P.;　Beh, E. S.;　Goulet, M. A.;　De Porcellinis, D.;　Aspuru-Guzik, A.;　Gordon, R. G.; Aziz, M. J., Alkaline Benzoquinone Aqueous Flow Battery for Large-Scale Storage of Electrical Energy. *Advanced Energy Materials* **2018,** *8* (8), 1702056.

14. Wang, C. X.;　Yang, Z.;　Wang, Y. R.;　Zhao, P. Y.;　Yan, W.;　Zhu, G. Y.;　Ma, L. B.;　Yu, B.;　Wang, L.;　Li, G. G.;　Liu, J.; Jin, Z., High-Performance Alkaline Organic Redox Flow Batteries Based on 2-Hydroxy-3-carboxy-1,4-naphthoquinone. *Acs Energy Letters* **2018,** *3* (10), 2404-2409.

15. Tong, L.;　Goulet, M.-A.;　Tabor, D. P.;　Kerr, E. F.;　De Porcellinis, D.;　Fell, E. M.;　Aspuru-Guzik, A.;　Gordon, R. G.; Aziz, M. J., Molecular Engineering of an Alkaline Naphthoquinone Flow Battery. *ACS Energy Letters* **2019,** *4* (8), 1880-1887.

16. Ji, Y.;　Goulet, M. A.;　Pollack, D. A.;　Kwabi, D. G.;　Jin, S.;　Porcellinis, D.;　Kerr, E. F.;　Gordon, R. G.; Aziz, M. J., A Phosphonate-Functionalized Quinone Redox Flow Battery at Near-Neutral pH with Record Capacity Retention Rate. *Advanced Energy Materials* **2019,** *9* (12), 1900039.

17. Jin, S.;　Jing, Y.;　Kwabi, D. G.;　Ji, Y.;　Tong, L.;　De Porcellinis, D.;　Goulet, M. A.;　Pollack, D. A.;　Gordon, R. G.; Aziz, M. J., A water-miscible quinone flow battery with high volumetric capacity and energy density. *ACS Energy Letters* **2019,** *4* (6), 1342-1348.

18. Hu, B.;　Luo, J.;　Hu, M.;　Yuan, B.; Liu, T. L., A pH-Neutral, Metal-Free Aqueous Organic Redox Flow Battery Employing an Ammonium Anthraquinone Anolyte. *Angew Chem Int* **2019,** *58* (46), 16629-16636.

19. Wu, M.;   Jing, Y.;   Wong, A. A.;   Fell, E. M.;   Jin, S.;   Tang, Z.;   Gordon, R. G.; Aziz, M. J., Extremely stable anthraquinone negolytes synthesized from common precursors. *Chem* **2020,** *6*, 11.

20. Jing, Y.;   Wu, M.;   Wong, A. A.;   Fell, E. M.;   Jin, S.;   Pollack, D. A.;   Kerr, E. F.; Gordon, R. G.; Aziz, M. J., In situ electrosynthesis of anthraquinone electrolytes in aqueous flow batteries. *Green Chemistry* **2020,** *22* (18), 6084-6092.

21. Wu, M.;   Bahari, M.;   Fell, E.;   Gordon, R. G.; Aziz, M. J., High-Performance Anthraquinone with Potentially Low Cost for Aqueous Redox Flow Batteries. *Journal of Materials Chemistry A* **2021**. https://doi.org/10.1039/D1TA08900E.

22. Liu, T. B.;   Wei, X. L.;   Nie, Z. M.;   Sprenkle, V.; Wang, W., A Total Organic Aqueous Redox Flow Battery Employing a Low Cost and Sustainable Methyl Viologen Anolyte and 4-HO-TEMPO Catholyte. *Advanced Energy Materials* **2015,** *6* (3), 1501449.

23. Hu, B.;   DeBruler, C.;   Rhodes, Z.; Liu, T. L., Long-Cycling Aqueous Organic Redox Flow Battery (AORFB) toward Sustainable and Safe Energy Storage. *J Am Chem Soc* **2017,** *139* (3), 1207-1214.

24. Beh, E. S.;   De Porcellinis, D.;   Gracia, R. L.;   Xia, K. T.;   Gordon, R. G.; Aziz, M. J., A Neutral pH Aqueous Organic-Organometallic Redox Flow Battery with Extremely High Capacity Retention. *ACS Energy Letters* **2017,** *2* (3), 639-644.

25. Luo, J.;   Hu, B.;   Debruler, C.; Liu, T. L., A pi-Conjugation Extended Viologen as a Two-Electron Storage Anolyte for Total Organic Aqueous Redox Flow Batteries. *Angew Chem Int Ed* **2018,** *57* (1), 231-235.

26. Hu, B.;   Tang, Y.;   Luo, J.;   Grove, G.;   Guo, Y.; Liu, T. L., Improved radical stability of viologen anolytes in aqueous organic redox flow batteries. *Chem Commun* **2018,** *54* (50), 6871-6874.

27. DeBruler, C.;   Hu, B.;   Moss, J.;   Luo, J.; Liu, T. L., A Sulfonate-Functionalized Viologen Enabling Neutral Cation Exchange, Aqueous Organic Redox Flow Batteries toward Renewable Energy Storage. *ACS Energy Letters* **2018,** *3* (3), 663-668.

21

369   28. Liu, Y. H.;   Goulet, M. A.;   Tong, L. C.;   Liu, Y. Z.;   Ji, Y. L.;   Wu, L.;   Gordon, R. G.;

370   Aziz, M. J.;   Yang, Z. J.; Xu, T. W., A Long-Lifetime All-Organic Aqueous Flow Battery Utilizing

371   TMAP-TEMPO Radical. *Chem* **2019,** *5* (7), 1861-1870.

372   29. Liu, W.;   Liu, Y.;   Zhang, H.;   Xie, C.;   Shi, L.;   Zhou, Y. G.; Li, X., A highly stable

373   neutral viologen/bromine aqueous flow battery with high energy and power density. *Chem*

374   *Commun* **2019,** *55* (33), 4801-4804.

375   30. Jin, S.;   Fell, E. M.;   Vina-Lopez, L.;   Jing, Y.;   Michalak, P. W.;   Gordon, R. G.; Aziz,

376   M. J., Near Neutral pH Redox Flow Battery with Low Permeability and Long-Lifetime

377   Phosphonated Viologen Active Species. *Advanced Energy Materials* **2020,** *10* (20), 2000100.

378   31. Liu, Y.;   Li, Y.;   Zuo, P.;   Chen, Q.;   Tang, G.;   Sun, P.;   Yang, Z.; Xu, T., Screening

379   Viologen Derivatives for Neutral Aqueous Organic Redox Flow Batteries. *ChemSusChem* **2020**,

380   13, 2245-2249.

381   32. Winsberg, J.;   Stolze, C.;   Muench, S.;   Liedl, F.;   Hager, M. D.; Schubert, U. S.,

382   TEMPO/Phenazine Combi-Molecule: A Redox-Active Material for Symmetric Aqueous Redox-

383   Flow Batteries. *ACS Energy Letters* **2016,** *1* (5), 976-980.

384   33. Hollas, A.;   Wei, X. L.;   Murugesan, V.;   Nie, Z. M.;   Li, B.;   Reed, D.;   Liu, J.;

385   Sprenkle, V.; Wang, W., A biomimetic high-capacity phenazine-based anolyte for aqueous organic

386   redox flow batteries. *Nature Energy* **2018,** *3* (6), 508-514.

387   34. Wang, C.;   Li, X.;   Yu, B.;   Wang, Y.;   Yang, Z.;   Wang, H.;   Lin, H.;   Ma, J.;   Li, G.;

388   Jin, Z., Molecular Design of Fused-Ring Phenazine Derivatives for Long-Cycling Alkaline Redox

389   Flow Batteries. *ACS Energy Letters* **2020,** *5* (2), 411-417.

390   35. Pang, S.;   Wang, X.;   Wang, P.; Ji, Y., Biomimetic Amino Acid Functionalized Phenazine

391   Flow Batteries with Long Lifetime at Near-Neutral pH. *Angew Chem Int Ed* **2021,** *60*, 5289 –5298

392   36. Lin, K.;   Gomez-Bombarelli, R.;   Beh, E. S.;   Tong, L.;   Chen, Q.;   Valle, A.;   Aspuru-

393   Guzik, A.;   Aziz, M. J.; Gordon, R. G., A redox-flow battery with an alloxazine-based organic

394   electrolyte. *Nature Energy* **2016,** *1* (9), 16102.

395   37. Zhao, Z.;   Zhang, B.;   Schrage, B. R.;   Ziegler, C. J.; Boika, A., Investigations Into

Aqueous Redox Flow Batteries Based on Ferrocene Bisulfonate. *ACS Applied Energy Materials* **2020,** *3* (10), 10270-10277.

38. Li, Y.; Xu, Z.; Liu, Y.; Jin, S.; Fell, E. M.; Wang, B.; Gordon, R. G.; Aziz, M. J.; Yang, Z.; Xu, T., Functioning water-insoluble ferrocenes for aqueous organic flow battery via host-guest inclusion. *ChemSusChem* **2021**, 14, 745 – 752

39. Winsberg, J.; Janoschka, T.; Morgenstern, S.; Hagemann, T.; Muench, S.; Hauffman, G.; Gohy, J. F.; Hager, M. D.; Schubert, U. S., Poly(TEMPO)/Zinc Hybrid-Flow Battery: A Novel, "Green," High Voltage, and Safe Energy Storage System. *Adv Mater* **2016,** *28* (11), 2238-43.

40. Goulet, M.-A.; Tong, L.; Pollack, D. A.; Tabor, D. P.; Odom, S. A.; Aspuru-Guzik, A.; Kwan, E. E.; Gordon, R. G.; Aziz, M. J., Extending the lifetime of organic flow batteries via redox state management. *J. Am. Chem. Soc.* **2019,** *141* (20), 8014-8019.

41. Wang, C.; Yu, B.; Liu, Y.; Wang, H.; Zhang, Z.; Xie, C.; Li, X.; Zhang, H.; Jin, Z., N-alkyl-carboxylate-functionalized anthraquinone for long-cycling aqueous redox flow batteries. *Energy Storage Materials* **2021,** *36*, 417-426.

42. Yan Jing, E. M. F., Min Wu, Shijian Jin, Yunlong Ji, Daniel A. Pollack, Zhijiang Tang, Dian Ding, Meisam Bahari, Marc-Antoni Goulet, Tatsuhiro Tsukamoto, Roy G. Gordon, Michael J.Aziz long-lifetime-potentially-low-cost-anthraquinone-flow-battery-chemistry-developed-from-study-of-effects-of-water-solubilizing-group-and-connection-to-core. *ChemRxiv* **2021,** (10.33774/chemrxiv-2021-0cb4d).

43. Petit, Y. K.; Mourad, E.; Prehal, C.; Leypold, C.; Windischbacher, A.; Mijailovic, D.; Slugovc, C.; Borisov, S. M.; Zojer, E.; Brutti, S.; Fontaine, O.; Freunberger, S. A., Mechanism of mediated alkali peroxide oxidation and triplet versus singlet oxygen formation. *Nat Chem* **2021**.

44. Marcus, R. A., Electron transfer reactions in chemistry. Theory and experiment. *Reviews of Modern Physics* **1993,** *65* (3), 599-610.

45. Goulet, M.-A.; Aziz, M. J., Flow Battery Molecular Reactant Stability Determined by

Symmetric Cell Cycling Methods. *Journal of the Electrochemical Society* **2018,** *165* (7), A1466-A1477.

46. McCann, G. M.;　McDonnell, C. M.;　Magris, L.; More O'Ferrall, R. A., Enol–keto tautomerism of 9-anthrol and hydrolysis of its methyl ether. *Journal of the Chemical Society, Perkin Transactions 2* **2002,**　(4), 784-795.

47. Liang, S.;　Subrahmanyam, A. V.;　Khadem, M.;　Zhao, Y.; Adronov, A., Selective dispersion of single-walled carbon nanotubes with electron-rich fluorene-based copolymers. *RSC Advances* **2016,** *6* (31), 25733-25740.

433 **Supporting information**

434 # A Highly Stable Low Redox Potential Quinone for Aqueous

435 # Flow Batteries

436 Min Wu,[1] Meisam Bahari,[1] Yan Jing,[2] Kiana Amini,[1] Eric M. Fell,[1] Thomas Y. George,[1] Roy G.

437 Gordon,[2]*Michael J. Aziz[1]*

438

Contents

465

466

Experimental Materials:

2,6-diaminoanthraquione (97%), 1,3-propanesultone (98%), sodium hydride (60% in mineral oil), anhydrous dimethyl sulfoxide, anhydrous N,N-Dimethylformamide, potassium carbonate, and palladium(II) acetate (98%) were purchased from Sigma-Aldrich. 2,6-dihydroxyanthraquinone (98%) was purchased from AK scientific. Sodium allylsulfonate (94%) was purchased from Ambeed, inc. Ltd. Hydrogen was purchased from Airgas. The materials were directly used without further purification.

Synthesis of 2,6-N-TSAQ

3 g of 2,6-diaminoanthraquinone (12.59 mmol) was added to 50 mL anhydrous dimethyl sulfoxide. Then 2.1 g sodium hydride (60%, 52.46 mmol) was added to the solution under vigorous stirring. After 15 minutes, 6.41 g 1,3-propanesultone (98%, 52.46 mmol) was added to the above mixture. The solution was stirred at room temperature for overnight. Afterward, ethyl acetate was added to the solution and collect the red solid. The crude product was further washed with ethyl acetate to remove any mineral oil. Yield:9.7 g (95%).

The ^{1}H NMR spectrum of 2,6-N-TSAQ is shown in Figure S1.
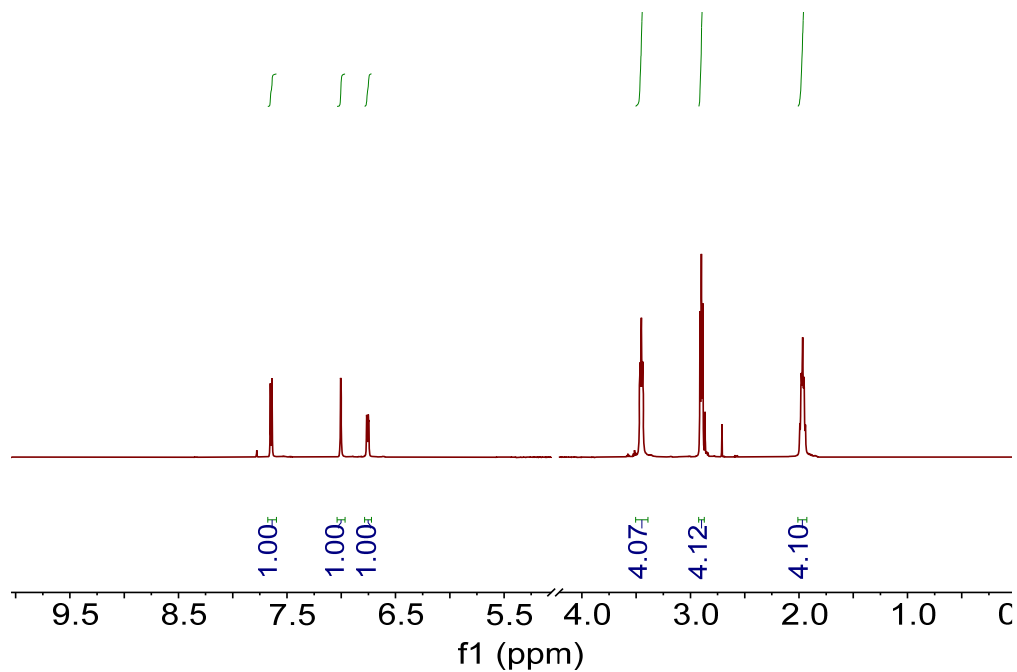
Figure S1. ^{1}H NMR spectrum of 2,6-N-TSAQ in D2O-d6. Solvent peak at 4.7 pm was censored to increase other peaks. ^{1}H NMR (500 MHz, D$_2$O) δ 7.65 (d, 2H), 7.00 (d, 2H), 6.76 (dd, 2H), 3.45 (t, 8H), 2.90 (t, 8H), 1.97 (m, 8H).
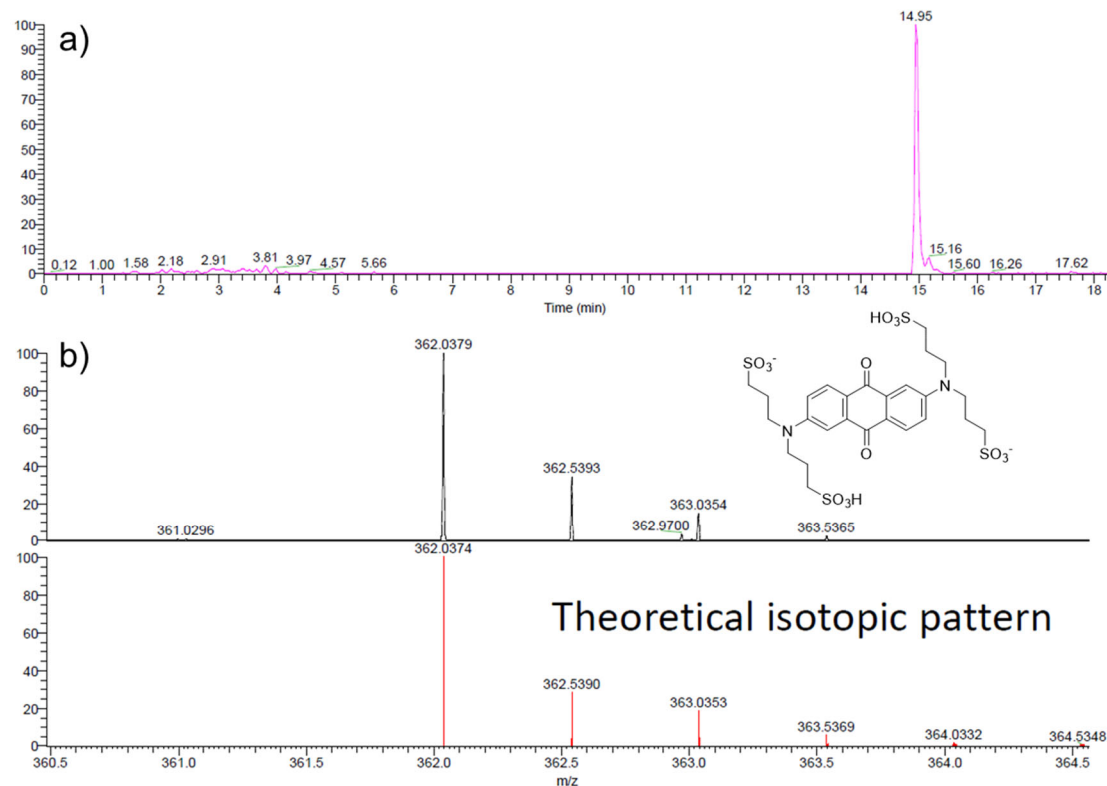
Figure S2. LC-MS traces of the synthesized 2,6-N-TSAQ. a) LC trace of 2,6-N-TSAQ; b) Mass

spectrum of the material eluted at 14.95 min in the LC trace. The peak at m/z = 362.04

corresponding to the 2,6-N-TSAQ with two protonate form and two negative charges. Sample

preparation: 0.1 M 2,6-N-TSAQ was diluted 100 times with HPLC water, and further diluted 100

times with acetonitrile/water co-solvents (V/V=1:1) to the desired concentration 10 μM. High-

resolution LC-MS analysis was performed in the Small Molecule Mass Spectrometry Facility at

Harvard University on a MiniLIMS. The elution solution is 0.1% v/v formic acid in acetonitrile.

The ESI mass spectrum was recorded in negative ionization mode.

Synthesis of 2,6-O-DPSAQ

3 g of 2,6-dihydroxyanthraquinone (12.49 mmol) was added to 50 mL anhydrous N,N-

Dimethylformamide. Then 1.05 g sodium hydride (60%, 26.23 mmol) was added to the solution

under vigorous stirring. After 15 minutes, 3.20 g 1,3-propanesultone (98%, 26.23 mmol) was

added to the above mixture. The solution was stirred at room temperature for overnight.

Afterwards, ethyl acetate was added to the solution to collect the yellow solid. The crude product

was washed with ethyl acetate to remove any mineral oil. Yield: 6.4 g (97%).

The ^{1}H NMR spectrum of 2,6-O-DPSAQ is shown in Figure S3.
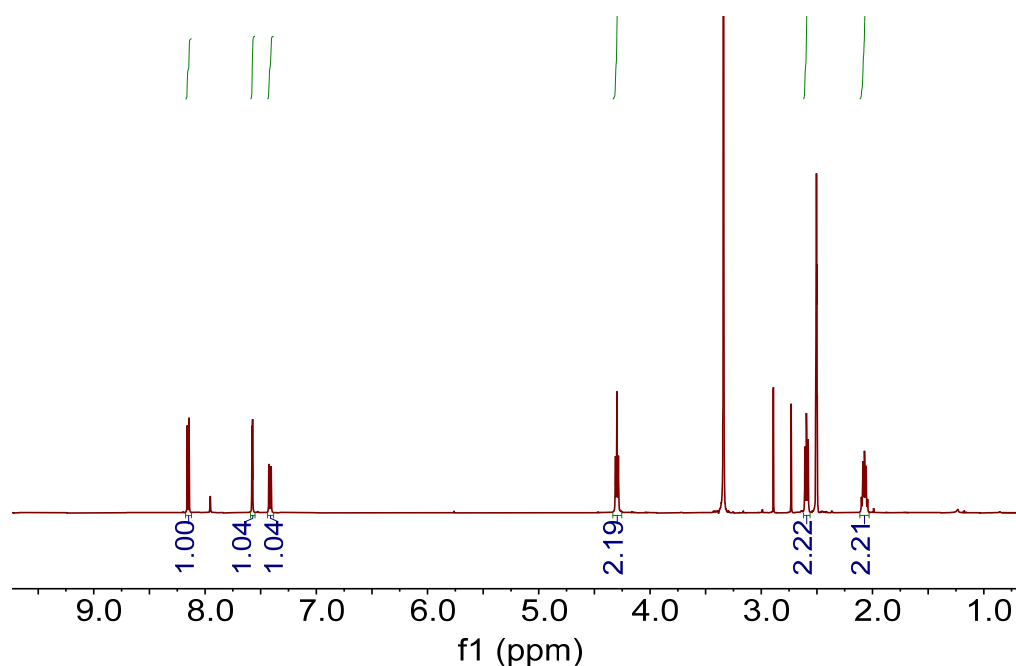
Figure S3. ^{1}H NMR spectrum of 2,6-O-DPSAQ in DMSO-d6. Solvent peaks are those not

integrated. ^{1}H NMR (500 MHz, DMSO-d6) δ 8.15 (d, 2H), 7.58 (d, 2H), 7.42 (dd, 2H), 4.30 (t,

4H), 2.59 (t, 4H), 2.07 (m, 4H).

510 **Synthesis of 2,6-DPSAQ**

511 2,6-diiodoanthraquinone was synthesized according to the reported procedure.[47]

512 Heat a mixture of 2 g 2,6-diiodoanthraquinone (4.35 mmol), 0.75 g sodium

513 allylsulfonate (5.22 mmol), 0.72 g potassium carbonate (5.22 mmol) and 49 mg

514 palladium acetate(0.22 mmol) in 40 mL water in a pressure vessel to 120 °C for

515 overnight. The mixture solution was filtered to remove insoluble gradients. Collect

516 the filtrate and add it to a 20 mL methanol. The solution was stirred in a hydrogen

517 atmosphere for overnight.

518 Evaporate the solution in vacuum to collect the solid. Yield: 1.51 g (70%).

519 The ^{1}H NMR spectrum of 2,6-DPSAQ is shown in Figure S4.
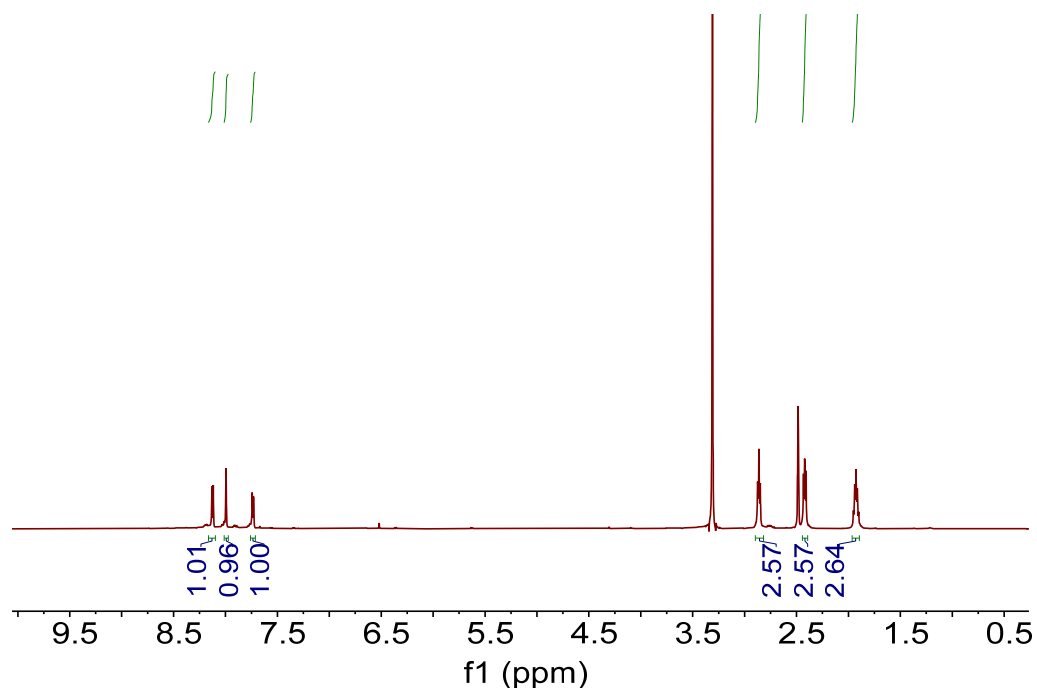
520

521 **Figure S4.** ^{1}H NMR spectrum of 2,6-DPSAQ in DMSO-d6. Solvent peaks are those not

522 integrated. ^{1}H NMR (500 MHz, DMSO-d6) δ 8.12 (d, 2H), 7.99 (d, 2H), 7.74 (dd, 2H), 2.86 (t,

523   4H), 2.42 (t, 4H), 1.93 (m, 4H).

524

Table S1. The lab-scale cost of 2,6-DHAQ, 2,6-DAAQ and 1,3-propanesultone are from Sigma-

Aldrich in July 2021.

Molecules	Lab-Scale Cost ($/Mol)
2,6-DHAQ	364
2,6-DAAQ	6918
1,3-propanesultone	77
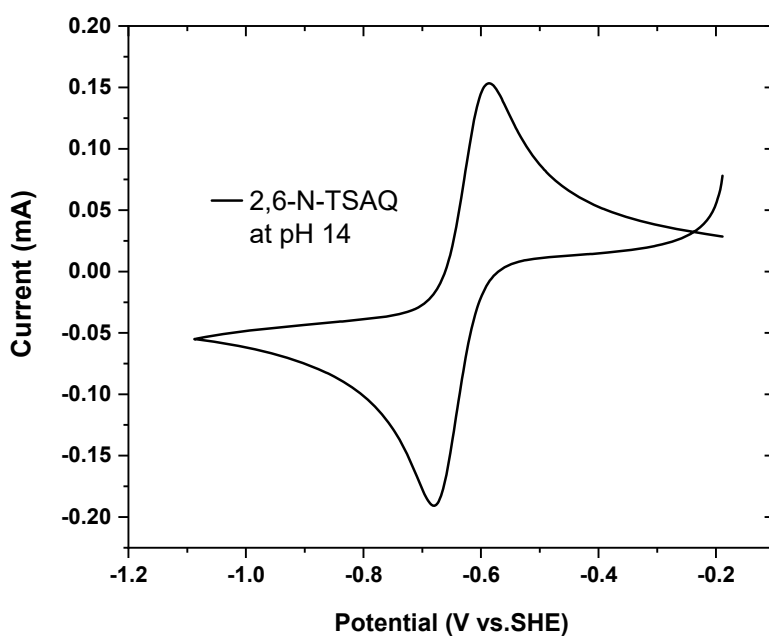
Figure S5. Cyclic voltammograms of 5 mM 2,6-N-TSAQ in 1 M sodium hydroxide at a scan rate

of 100 mV/s.

UV-vis and permeability measurements

UV-vis absorbance spectra for calibration curves and crossover detection were taken using an Agilent 8453 spectrophotometer. The permeability of 2,6-N-TSAQ through Nafion NR212 cation exchange membrane was measured in a custom two-compartment diffusion cell ("H-cell") made by Adams & Chittenden scientific glassware. The Nafion NR212, received protonated, was ion exchanged to sodium form in 1 M NaOH by soaking for over 12 hours at ambient temperature. This membrane was sealed between a donating compartment containing 10 mL of 0.1 M 2,6-N-TSAQ in 1 M NaOH and a receiving compartment containing 10 mL of 0.17 M Na_2SO_4 in 1 M NaOH. The electrolyte in the receiving compartment was designed to minimize osmotic pressure gradients influencing permeability: a freezing point osmometer (Advanced Instruments Inc., Model 3300) confirmed the osmolarity difference between the compartments was only 0.018 Osm. Both compartments were stirred continuously using magnetic stir bars.

Three identical H-cells stirred for 13 days, and 2 mL aliquots were periodically removed from the receiving side to measure absorbance spectra, which were then replaced with fresh receiving solution. Due to the exceptionally low crossover rate, the spectrophotometer was unable to detect the peaks characteristic of 2,6-N-TSAQ, so an upper limit was assigned based on the highest absorbance value observed at 455 nm during the experiment (Fig S8). Using the derivation of Fick's Law reported previously,[1] 2,6-N-TSAQ cannot exceed 3×10^{-14} cm^2/s under these conditions.
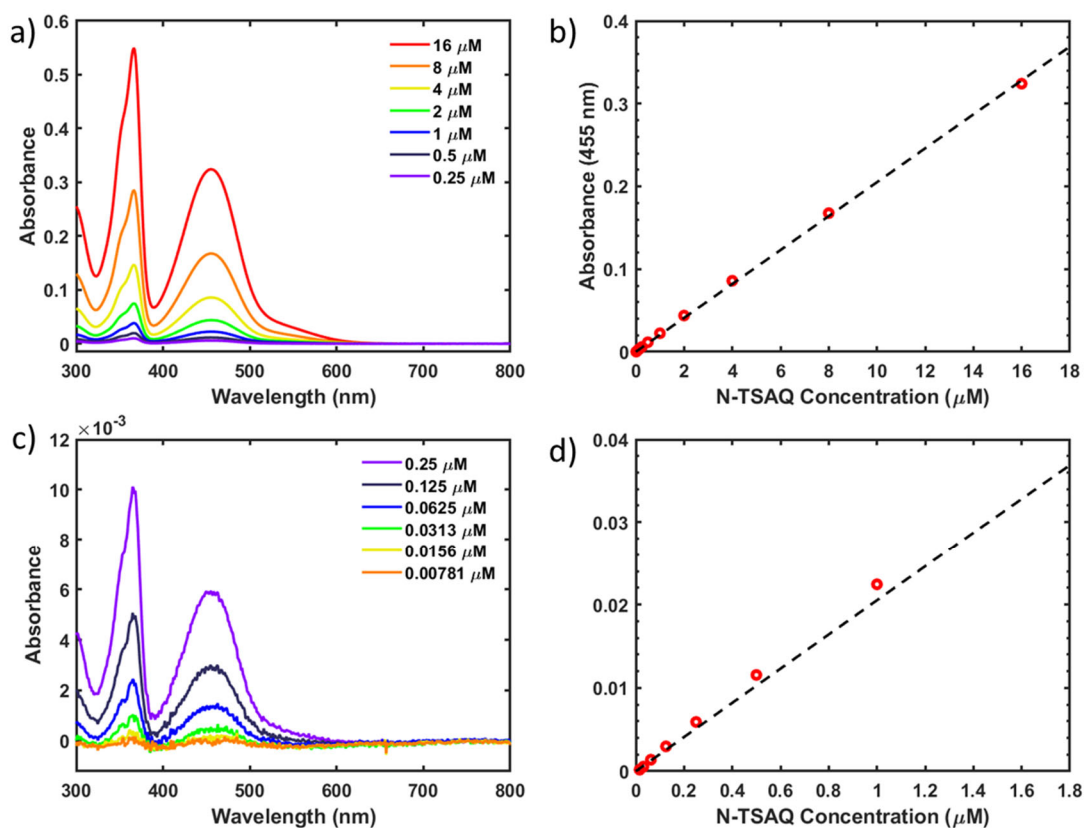
Figure S6. UV-vis absorbance spectra for 2,6-N-TSAQ at concentrations of a) 16 μM to 0.25

μM and c) 0.25 μM to 0.00781 μM in 1 M NaOH. Solutions were prepared by serial 2:1 dilution

approaching the detection limit of the spectrophotometer. A baseline of zero absorbance at 750

nm was applied to all spectra. The slope of the resulting calibration curve in panels b) and d)

(10x zoom in to the origin of b) gives a molar attenuation coefficient of 0.0205 μM^{-1}cm^{-1}.

559
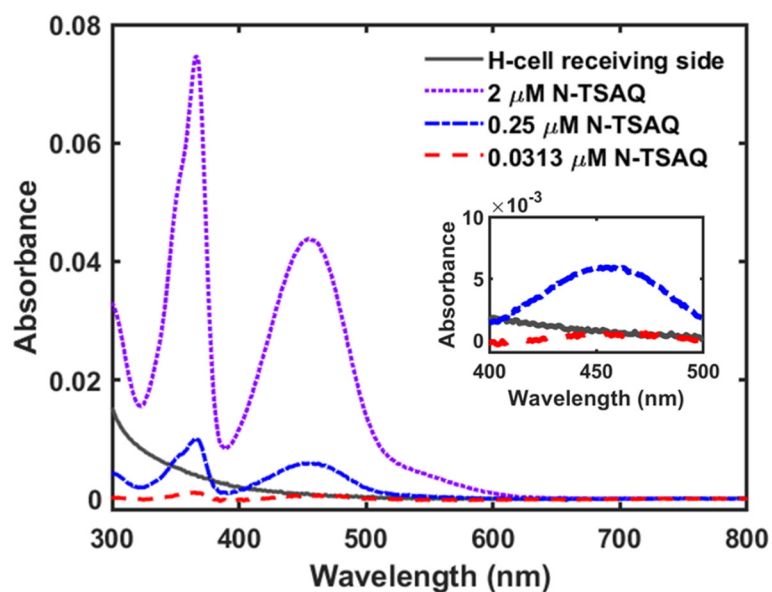
Figure S7. UV-vis of H-cell measurement. The grey trace is the UV-vis absorbance spectrum of

the receiving solution of a two-compartment diffusion H-cell which exhibited the highest

absorbance at 455 nm over 13 days. This absorbance was used to calculate an upper limit on the

permeability of 2,6-N-TSAQ through Nafion NR212 because the peaks indicative of 2,6-N-

TSAQ were not detectable by the spectrophotometer. Therefore, the permeability cannot be

greater than 3 $\times$ 10^{-14} cm^2/s. The small absorbance at 300-400 nm indicates a minor impurity

which does not interfere with the 2,6-N-TSAQ peak at 455 nm.

567
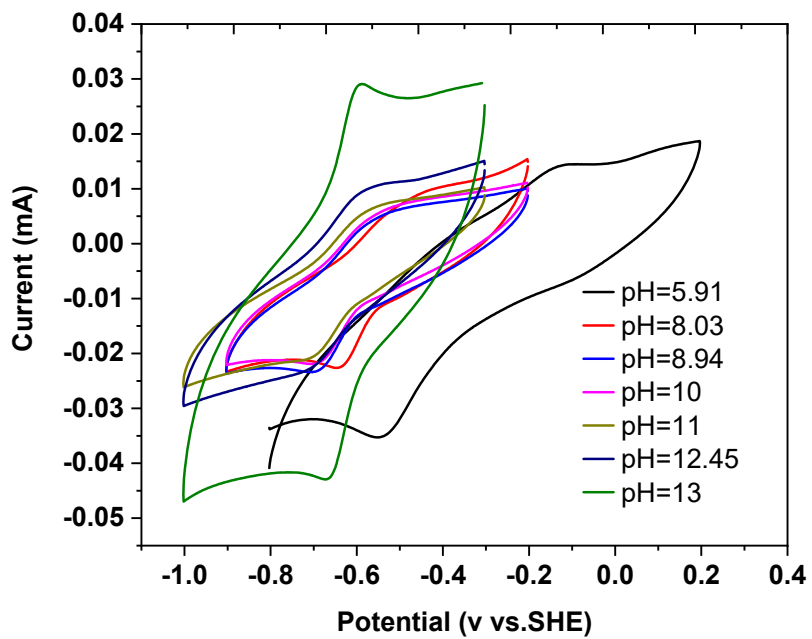
Figure S8. CV of 2 mM 2,6-N-TSAQ in different pH buffer solutions at a sweep rate of 100 mV/s.
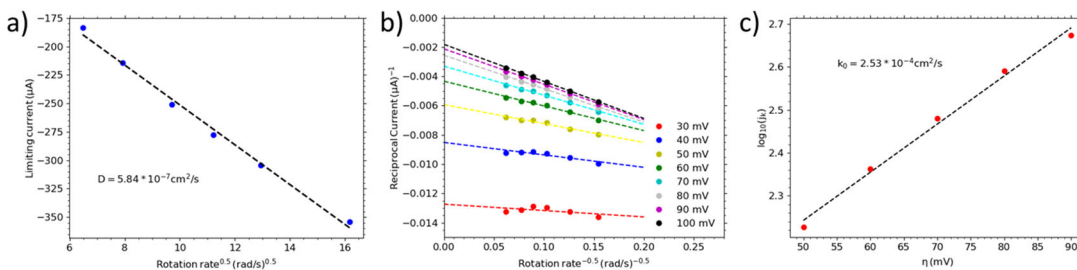
Figure S9. Electrochemical kinetics of 2,6-N-TSAQ in 1 M NaOH. a) Levich plot (limiting current versus square root of rotation rate) of 5 mM 2,6-N-TSAQ in 1 M NaOH. Limiting current is taken as the current at -0.8 V vs SHE in Figure 3b. The slope yields a diffusion coefficient for the 2,6-N-TSAQ of 5.84×10^{-7} cm^2/s; b) Koutecký-Levich plot (reciprocal current versus inverse square root of rotation rate) of 5 mM 2,6-N-TSAQ in 1 M NaOH; c) Fitted Tafel plot of 5 mM 2,6-N-TSAQ in 1 M NaOH. The charge transfer coefficient is calculated to be 0.32, and the rate constant is calculated to be 2.53×10^{-4} cm/s.

Full cell measurements

Flow battery experiments were performed with cell and hardware from Fuel Cell Tech.

(Albuquerque, NM). Pyrosealed POCO graphite flow plates with serpentine flow designs were

used for both electrodes. Each electrode comprised a 5 cm^2 geometric surface area enclosed by

one piece of AvCarb carbon electrode. For 2,6-N-TSAQ/ferrocyanide full cell tests, a Nafion^{TM}

212 membrane was used to serve as the ion-selective membrane. The Nafion membrane was

soaked in the supporting electrolyte (sodium hydroxide or sodium chloride) for at least 24 hours

before use. Viton sheets were used to cover the outer portion space between the electrodes.

Torque used for cell assembly was 60 lb-in (6.78 Nm) on each of eight 1/4-28 bolts. The

electrolytes were input into the cell through fluorinated ethylene propylene (FEP) tubing at a rate

of 60 mL/min, controlled by Cole-Parmer 6 Masterflex L/S peristaltic pumps. The cell was run

inside a glove box (1 ppm O_2). Cell polarization measurements and charge-discharge cycling

were conducted using a Biologic BCS-815 battery cycler. Long-term cycling of the 0.1 M 2,6-N-

TSAQ/ferrocyanide cell was achieved at ±40 mA cm^{-2} with potential holds at 1.4 V for charging

and 0.6 V for discharging until the current density dropped to 2 mA cm^{-2}. The polarization

curves were obtained by charging to a desired state of charge first and then polarizing via linear

sweep voltammetry at a rate of 100 mV s^{-1}.

A glassy carbon (BASi, 3 mm diameter) working electrode, an Ag/AgCl reference electrode

(BASi, 3 M NaCl solution), and a graphite counter electrode were used in the three-electrode
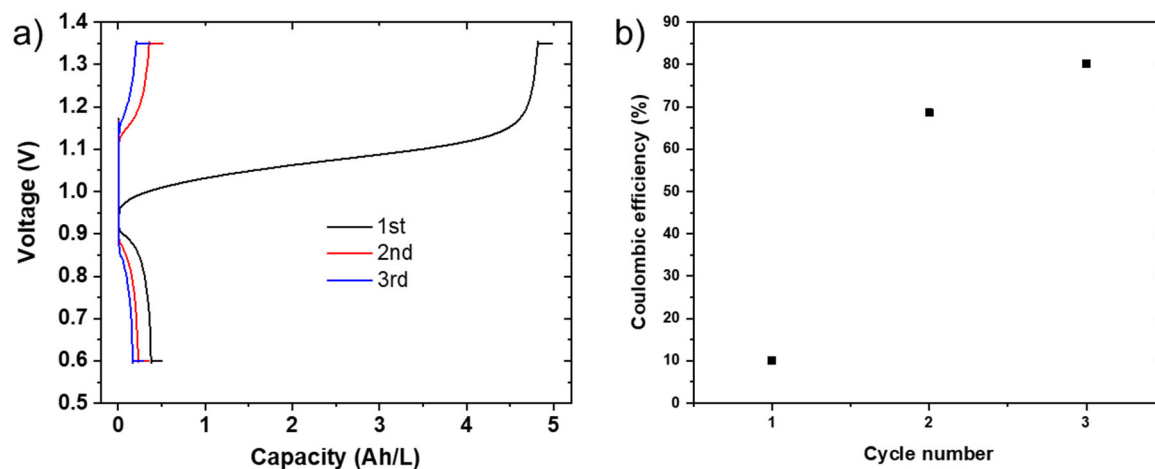
system for all CV tests.

601

602
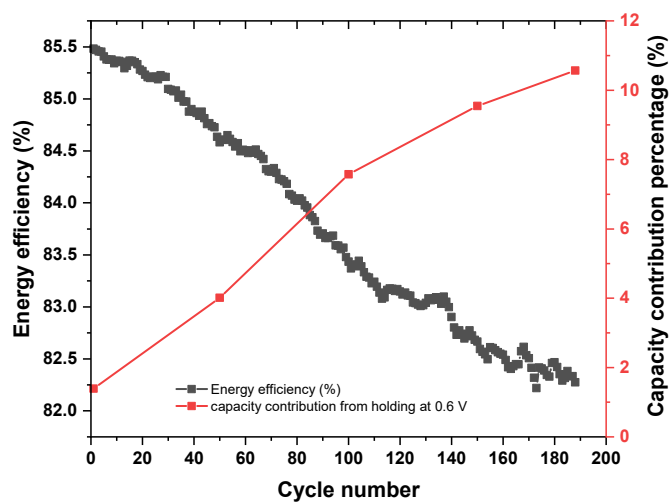
Figure S10. Energy efficiency and capacity contribution percentage at voltage hold at 0.6 V

versus cycle number of the 0.1 M 2,6-N-TSAQ/ferrocyanide cell in 1 M sodium chloride

solution.

606

Figure S11. Cell performance of 0.1 M 2,6-N-TSAQ/ferrocyanide cell in 1M NH$_4$Cl supporting

electrolyte. a) Charge-discharge voltage profile of 0.1 M 2,6-N-TSAQ/ferrocyanide full cell in 1

M NH$_4$Cl at pH 7. b) The corresponding coulombic efficiency for 0.1 M 2,6-N-

TSAQ/ferrocyanide cell in 1 M NH$_4$Cl condition. Cell condition: 5 mL 0.1 M 2,6-N-TSAQ in 1

M NH$_4$Cl as the negolyte, and 30 mL 0.1 M K$_4$Fe(CN)$_6$ and 0.02 M K$_3$Fe(CN)$_6$ in 1 M NH$_4$Cl as

the posolyte, both electrolytes are tuned to pH 7 with sodium hydroxide.
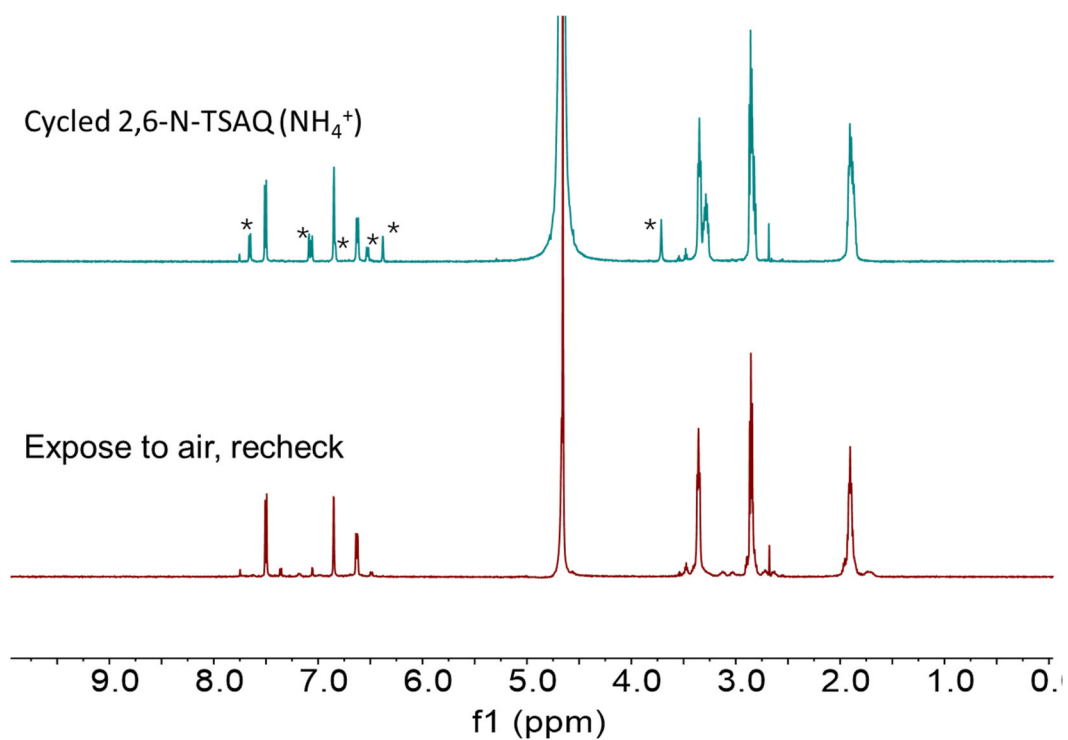
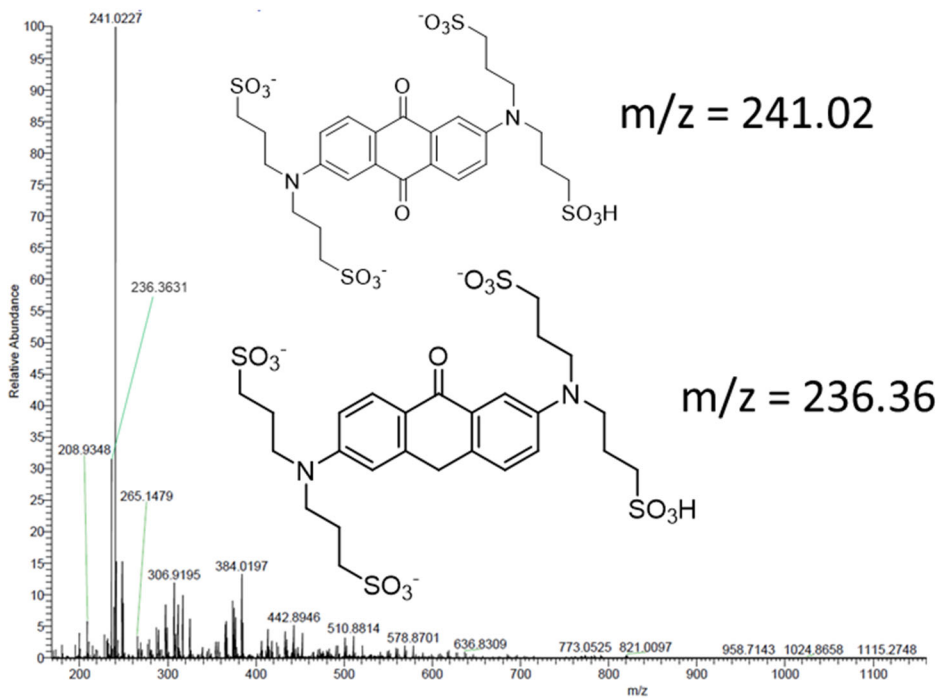**Figure S12.** ^{1}H NMR spectra (500 MHz) of the cycled 2,6-N-TSAQ in 1 M NH$_4$Cl electrolyte diluted with 5 volumes of D$_2$O solvent. The asterisk peaks belong to anthrone, after fully air aerated, the anthrone peaks disappeared.
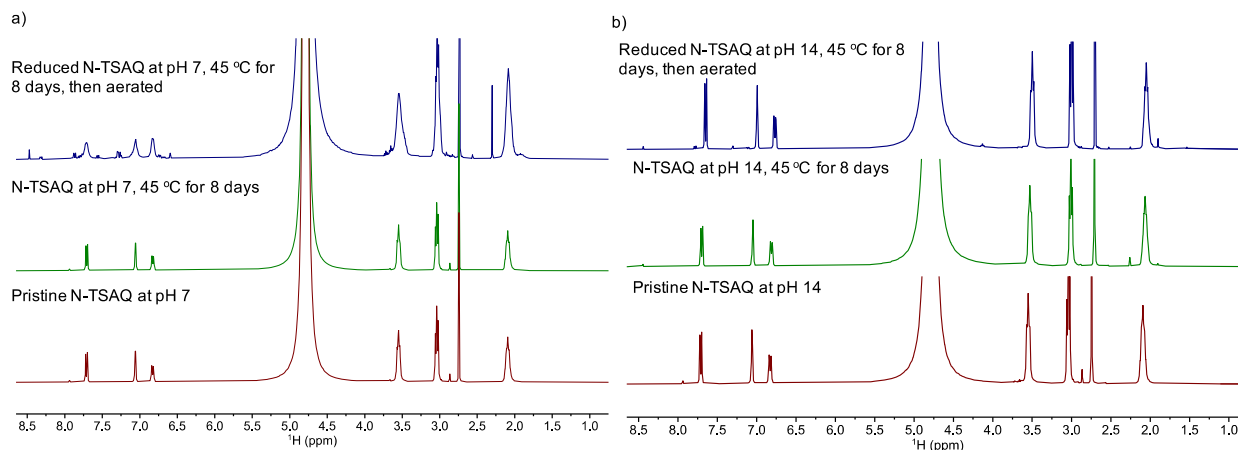
622

Figure S13. The mass spectrum of the cycled 2,6-NTSAQ (NH$_4$Cl) electrolyte. The electrolyte was diluted 10,000 times with HPLC water and directly analyzed with mass spectrometry. The m/z peak at 236.36 belongs to the anthrone peak, and peak at 241.02 belong to 2,6-N-TSAQ.

Figure S14. ^{1}H NMR spectra (400 MHz) of 2,6-N-TSAQ in D$_2$O solvent. (a) from bottom to top: pristine 2,6-N-TSAQ; 0.1 M 2,6-N-TSAQ in 1 M NaCl at 45 °C for 8 days; 0.1 M reduced form of 2,6-N-TSAQ in 1 M NaCl at 45 °C for 8 days, then aerated; (b) from bottom to top: pristine 2,6-N-TSAQ; 0.1 M 2,6-N-TSAQ in 1 M NaOH at 45 °C for 8 days; 0.1 M reduced form of 2,6-N-TSAQ in 1 M NaOH at 45 °C for 8 days, then aerated.

References

1. Kwabi, D. G.; Lin, K.; Ji, Y.; Kerr, E. F.; Goulet, M.-A.; De Porcellinis, D.;

Tabor, D. P.; Pollack, D. A.; Aspuru-Guzik, A.; Gordon, R. G.; Aziz, M. J.,

Alkaline quinone flow battery with long lifetime at pH 12. *Joule* **2018,** *2* (9),

1907-1908.